Elastic Depolarization of OH(A) by He and Ar: A Comparative Study

ARTICLE *in* THE JOURNAL OF PHYSICAL CHEMISTRY A · SEPTEMBER 2009

Impact Factor: 2.69 · DOI: 10.1021/jp905348c · Source: PubMed

Elastic Depolarization of OH(A) by He and Ar: A Comparative Study[†]

M. L. Costen, R. Livingstone, K. G. McKendrick,* and G. Paterson

School of Engineering and Physical Sciences, Heriot-Watt University, Edinburgh, EH14 4AS, United Kingdom

M. Brouard,[‡] H. Chadwick, Y.-P. Chang, and C. J. Eyles

The Department of Chemistry, University of Oxford, The Physical and Theoretical Chemistry Laboratory, South Parks Road, Oxford, OX1 3QZ, United Kingdom

F. J. Aoiz[§]

Departamento de Química Física, Facultad de Química, Universidad Complutense, 28040 Madrid, Spain

J. Kłos[||]

Department of Chemistry and Biochemistry, University of Maryland, College Park, Maryland 20742

Received: June 7, 2009; Revised Manuscript Received: August 5, 2009

Two color polarization spectroscopy has been employed to measure the collisional depolarization of OH($A^2\Sigma^+$, $v = 1$) by He and Ar. Complementary experiments using Zeeman quantum beat spectroscopy have also been performed to determine separately the cross sections for rotational energy transfer (RET) out of selected rotational levels of OH(A, $v = 0$) + Ar, as well as those for elastic depolarization. This has been achieved by dispersing the emission, so as to observe a single fluorescence transition. Elastic depolarization of OH(A) by Ar is found to be significant with that for loss of rotational alignment exceeding that for loss of orientation. In the case of OH(A) + He, the polarization spectroscopy measurements suggest that elastic depolarization plays a relatively minor role in the loss of the polarization signal compared with RET. The experimental data for OH(A) + Ar are compared in detail with the results of quasi-classical trajectory calculations that accommodate the effects of electron spin. These classical calculations are assessed against the results obtained using full close-coupled open shell quantum mechanical scattering methods. Overall the level of agreement between the two experiments, and between experiment and theory, is very reasonable. Surprisingly, at low N the elastic depolarization cross sections for OH(A) + Ar are found to be quite similar in magnitude to those observed for OH(X) + Ar despite the fact that the well depth in the latter system is considerably smaller than that for OH(A)−Ar. However, for OH(A) + Ar the depolarization cross sections are insensitive to N in the range 1−14. It is proposed that this behavior partly reflects the relatively anisotropic nature of the potential energy surface, which exhibits deep wells of different depths at the two linear configurations OH(A)−Ar and Ar−OH(A), and partly the nature of elastic depolarizing collisions, which must occur with a velocity component perpendicular to the plane of rotation of the diatomic molecule.

I. Introduction

There has been considerable interest in recent years in collisions that bring about a change in the direction of the angular momentum of a molecule.[1] These (de)polarizing collisions may accompany both elastic or inelastic scattering events, and their study in simple atom−diatom systems provides valuable clues about the vector properties in more complex reactive systems.[1−7] Elastic and inelastic collisions between atoms and open shell molecules have been a particular focus of study,[8,9] since these systems possess a richer electronic structure than in the closed shell case, yet are still amenable to experimental and theoretical study in exquisite detail.[1,10] The focus of the present work is the angular momentum depolarization that can be induced by elastic collisions.

In addition to the elegant crossed molecular beam studies of collision-induced rotational orientation and alignment cited above,[1,6,7] there have been a number of new spectroscopic methods developed recently to probe angular momentum polarization effects in chemical processes.[9] Two of these techniques, polarization spectroscopy (PS)[11−16] and Zeeman quantum beat spectroscopy (ZQBS)[17−19] have been employed to study the collisional angular momentum depolarization of simple diatomic radicals with a variety of collision partners. ZQBS, in which the angular momentum depolarization is manifest in the time dependent Zeeman quantum beat amplitude, has mainly been applied to the collisional depolarization of electronically excited radicals such as OH($A^2\Sigma^+$)[17−19] and NO($A^2\Sigma^+$).[19,20] Thus far, these experiments have focused on the measurement of total depolarization cross sections, that is, the sum of the depolarization caused by elastic and inelastic collisions. The complementary technique of two color polariza-

[†] Part of the "Vincenzo Aquilanti Festschrift".

* To whom correspondence should be addressed. E-mail: k.g.mckendrick@hw.ac.uk.

[‡] E-mail: mark.brouard@chem.ox.ac.uk.

[§] E-mail: aoiz@quim.ucm.es.

[||] E-mail: jklos@umd.edu.

10.1021/jp905348c
Published on Web 09/16/2009

tion spectroscopy (TCPS) has to date been used to study the depolarization accompanying elastic scattering and has been applied mainly to the study of collisions of OH($X^2\Pi$) radicals with rare gases and simple molecules.[11−16] In the present work, we report a coordinated study using both of these techniques to investigate in detail the collisional depolarization of OH(A) radicals with He and Ar. For the latter system in particular, this combined approach has allowed a full decomposition of the scattering process into depolarization accompanying elastic and inelastic, rotational energy transfer (RET) collisions.

The outline of the paper is as follows. Section II describes the theoretical and experimental procedures employed, and the methods used to analyze the TCPS and ZQBS experiments. In Section III, we present the OH($A^2\Sigma^+$) + Ar and He state-selected angular momentum depolarization rate coefficients at 300 K and velocity-averaged cross sections. Thermally averaged cross sections for RET are also reported. A detailed comparison of the results from the two experimental studies is made, as well as between experiment and the results of quasi-classical trajectory (QCT) theoretical calculations. The latter comparison allows a very detailed assessment to be made of the recently developed ab initio potential energy surface (PES) for OH($A^2\Sigma^+$) + Ar by Kłos et al.[21] In Section IV, we discuss the elastic depolarization behavior observed in OH(A) + He and Ar in the light of previous work on the collisional depolarization of OH(X) with Ar and He,[11−16] and measurements of the total depolarization cross sections for OH(A) + Ar.[17,21,22] The final section summarizes our principal conclusions.

II. Method

A. Calculation Details. ***1. Notation.*** As previously,[17,21,22] we employ the following notation. $\boldsymbol{N}$ ($\boldsymbol{N}'$) denotes the initial (final) state diatomic rotational angular momentum apart from electron and nuclear spin. For a diatomic radical in a $^2\Sigma^+$ electronic state for which electronic orbital angular momentum is zero, $\boldsymbol{N}$ ($\boldsymbol{N}'$) is equivalent to the nuclear rotational angular momentum, which must lie perpendicular to the internuclear axis, $\boldsymbol{r}$. The corresponding quantum number is written N (N'). The total rotational angular momentum apart from nuclear spin of OH($A^2\Sigma^+$) is denoted by $\boldsymbol{j}$, and its quantum number as j. Note that in cases in which OH(A) is treated as a closed shell species, $N = j$. In the Hund's case (b) coupling scheme appropriate for OH(A), the molecular wave function is defined by $\boldsymbol{j} = \boldsymbol{N} + \boldsymbol{S}$, where $\boldsymbol{S}$ is the electronic spin. The reactant and product quantum numbers F and F' are associated with the total diatomic angular momentum, including both electron and nuclear spin, that is, $\boldsymbol{F} = \boldsymbol{j} + \boldsymbol{I}$. The total angular momentum quantum number of the collision system (i.e., OH(A) + Ar/He in the application discussed in Sections II and III) is denoted by J and its projection onto the space fixed Z axis by M_J.

2. General Theory. The quantities measured in the present experiments are collisional depolarization rate constants, which can be converted into velocity averaged cross sections (see below). These depolarization cross sections can be thought of as measures of the $\boldsymbol{j}$-$\boldsymbol{j}'$ vector correlation,[2,3,22,23] which quantifies the tilt of the angular momentum subsequent to a collision. In both the classical and quantal descriptions of collisional depolarization, it is possible to relate the polarization moments after a collision, $\boldsymbol{P}_q^{(k)}(j')$, to the extrinsic moments of the initial state, $r_q^{(k)}(j)$, related to the preparation of j in the laboratory (LAB) frame, by[2,22,23]

$$\boldsymbol{P}_q^{(k)}(j') = a^{(k)}(j,j')r_q^{(k)}(j) \tag{1}$$

This equation is valid provided neither the initial nor the final directions of motion are defined. Classically, it is readily shown that the depolarization moments (or multipole transfer coefficients), $a^{(k)}(j,j')$, are directly related to the $\boldsymbol{j}$-$\boldsymbol{j}'$ vector correlation by the probability density function[22]

$$P(\theta_{jj'}) = \frac{1}{2}\sum_k [k]a^{(k)}(j,j')P_k(\cos\theta_{jj'}) \tag{2}$$

where $[k] \equiv (2k+1)$, $P_k(\cos\theta_{jj'})$ is the k^{th} Legendre polynomial, and the depolarization moments are defined as

$$a^{(k)}(j,j') = \langle P_k(\cos\theta_{jj'})\rangle \tag{3}$$

The quantum mechanical calculation of the depolarization moments has been discussed in detail in a number of papers.[2,22−26] When the initial and final directions of motion are unresolved, the multipole transfer coefficients are defined[2,3,22−29]

$$a^{(k)}(j,j') = [k]\frac{S_{qq}^{(kk)}(j,j')^*}{S_{00}^{(00)}(j,j')} = \frac{\sigma^{(kk)}(j,j')}{\sigma^{(00)}(j,j')} \tag{4}$$

where $\sigma^{(kk)}(j,j')$ appearing in eq 4 are the tensor cross sections of Alexander and Davis and Follmeg et al.,[2,23−26] while $S_{qq}^{(kk)}(j,j')^*$ are the correlation coefficients defined by Miranda and co-workers.[27−29] Expressions relating these coefficients to the scattering $\boldsymbol{T}$-matrix elements have been presented by a number of authors.[2,3,23−25]

We have shown previously that at fixed relative velocity, v_r, the bimolecular rate constants for collisional depolarization are given by[17]

$$k_{j\to j'}^{(k)} = k_{j\to j'}[1 - a^{(k)}(j,j')] = v_r\sigma_{j\to j'}(v_r)[1 - a^{(k)}(j,j')] \tag{5}$$

where $k_{j\to j'}$ and $\sigma_{j\to j'}(v_r)$ are the collision rate constants and cross sections, respectively. Note that the depolarization rate constants and cross sections are related by $k_{j\to j'}^{(k)} = v_r\sigma_{j\to j'}^{(k)}$. The quantum mechanical derivation of this expression has been presented recently by Dagdigian and Alexander.[24] In terms of the tensor cross sections of eq 4 we can write the depolarization cross sections[24,25]

$$\sigma_{j\to j'}^{(k)} = \sigma_{j\to j'}(v_r)[1 - a^{(k)}(j,j')] = ([j']/[j])^{1/2}[\sigma^{(00)}(j,j') - \sigma^{(kk)}(j,j')] \tag{6}$$

If the total collision rate constants are known, the measurement of the depolarization rate constants therefore allows direct evaluation to be made of the $\boldsymbol{j}$-$\boldsymbol{j}'$ vector correlation, as quantified by the $a^{(k)}(j,j')$ expansion coefficients. From the classical definition of the polarization parameters, eq 3, it is clear that $a^{(2)}(j,j')$ must lie within the limits $-1/2 \le a^{(2)}(j,j') \le 1$, and consequently the alignment depolarization rate constants are bounded by $1^1/_2 k_{j\to j'} \ge k_{j\to j'}^{(2)} \ge 0$. Therefore, when $a^{(2)}(j,j')$ is negative, the depolarization rate constant can exceed the collision rate constant. Similarly, since $a^{(1)}(j,j')$ ranges from $-1 \le a^{(1)}(j,j') \le 1$, the orientation depolarization rate constants must lie between $2k_{j\to j'} \ge k_{j\to j'}^{(1)} \ge 0$. These equations provide a convenient link between the measured depolarization rate

constants, and the dynamically interesting $\boldsymbol{j}$-$\boldsymbol{j}'$ depolarization parameters, $a^{(k)}(j,j')$. The limits on the quantum mechanical $a^{(k)}(j,j')$ parameters can differ from the values given above at low N, as has been discussed in general terms previously.[22]

The present experiments are conducted under thermal conditions, and hence the measured quantities are averages over a 300 K Maxwell−Boltzmann distribution of relative velocities. The velocity averaged value of $a^{(k)}(j,j')$ can then be written as[17]

$$\langle a^{(k)}(j,j')\rangle = \frac{\langle v_r \sigma_{j\rightarrow j'}(v_r) a^{(k)}(j,j';v_r)\rangle}{\langle v_r \sigma_{j\rightarrow j'}(v_{rel})\rangle} \quad (7)$$

such that

$$\langle k^{(k)}_{j\rightarrow j'}\rangle = \langle k_{j\rightarrow j'}\rangle[1 - \langle a^{(k)}(j,j')\rangle] \quad (8)$$

In the case of elastic depolarization, which is of most relevance to the present work, j should replace j' in the above equations.

Finally, for clarity we define here a simplified notation for the pure elastic depolarization rate constants, $k^{(k)} \equiv \langle k^{(k)}_{j\rightarrow j}\rangle$, and thermally (300 K) averaged cross sections, $\sigma^{(k)} \equiv \langle \sigma^{(k)}_{j\rightarrow j}\rangle$. Note that all of the experimental cross sections presented are thermally averaged values, and we therefore drop the angular bracket notation. The present article focuses specifically on the depolarization cross sections with $k = 1$ and $k = 2$, representing loss of orientation and alignment, respectively.

3. QM Method. Fully quantum close-coupling scattering calculations for OH(A) + Ar were performed using the new ab initio potential energy surface of Kłos et al.[21] This PES employs a fixed OH(A) bond length set equal to its equilibrium value, $r_e = 1.9126a_0$. As in our previous work,[17,21,22] the open shell (o-s) electronic structure of the OH(A) molecule was taken into account in the quantum mechanical (QM) scattering calculations using the HIBRIDON suite of codes,[30] which uses the Log-Derivative propagator by Manolopoulos and Alexander.[31,32] For the closed shell calculations of the integral cross sections, we employed the MOLSCAT code.[33]

In the close-coupling scattering calculations for the closed shell OH(A) + Ar system, the propagation was performed from 5 to 60 bohr. The rotational basis of OH(A) ranged up to $N = 14$ for total energies up to 330 cm^{-1}, and $N = 17$ for total energies up to 730 cm^{-1}. Twenty-five radial steps were used in the log-derivative integration. The total angular momentum was set automatically in MOLSCAT to converge the cross sections. For the highest total energies, it was necessary to include partial waves up to $J = 310$ for OH(A) + Ar. The open shell close-coupling QM scattering calculations were performed with similar convergence and basis parameters as in the case of the closed shell calculations.

4. QCT Method. The QCT procedure employed to calculate the depolarization cross sections follows that recently described in detail and applied to OH(A) + Ar,[22] and will only be described briefly here. Batches of approximately 1×10^5 trajectories were run for several initial N states at a fixed collision energy of 39 meV. This collision energy corresponds to the mean of a thermal distribution at 300 K (i.e., $\langle E_{coll}\rangle = (3/2)k_B T$). Since the PES for OH(A) + Ar has only been calculated for OH(A) at its equilibrium internuclear distance,[21] the method of Lagrange multipliers was used to force rigid rotor behavior during the integration of the classical equations of motion.[34] To assign the final state for each trajectory, the square of the rotational angular momentum $|\boldsymbol{N}'|^2 = N'(N'+1)\hbar^2$ was first calculated, and then the values of N' thereby obtained were rounded to the nearest integer. The Gaussian binning procedure (which involves weighting more heavily those trajectories with the "correct" rotational action)[35,36] was also applied in order to determine the state-to-state ($N \rightarrow N'$) cross sections, but the results were essentially indistinguishable from those obtained using the conventional histogram-binning procedure (i.e., rounding to the nearest integer). Trajectories whose final N' state were found to lie between $N \pm 0.5$ were considered elastic.

At a fixed collision energy, the expression for the inelastic cross-section is

$$\sigma_{N\rightarrow N'}(E_{coll}) = \pi b^2_{max}\frac{\mathcal{N}_{N'}}{\mathcal{N}_{tot}} \quad (9)$$

where $\mathcal{N}_{N'}$ is the number of trajectories ending in state N', and $\mathcal{N}_{tot}$ is the total number of trajectories (elastic plus inelastic). The maximum impact parameter leading to inelastic trajectories was determined by monitoring the change in the rotational quantum number, ΔN, with the criterion that no trajectories with $\Delta N > 0.5$ took place for $b > b_{max}$. Equation 9 implies that the impact parameter for the i-th trajectory is sampled according to $b^{(i)} = \xi^{1/2} b_{max}$, where ξ is a random number in the (0,1) interval.

The QCT calculation of the $a^{(k)}(N,N')$ polarization parameters consists simply of determining for each trajectory the asymptotic angle between the initial $\boldsymbol{N}$ and final $\boldsymbol{N}'$ angular momentum vectors[22]

$$\cos\theta_{NN'} = \frac{\boldsymbol{N}\cdot\boldsymbol{N}'}{|\boldsymbol{N}||\boldsymbol{N}'|} \quad (10)$$

The (de)polarization moments $a^{(k)}(N,N')$ are then calculated as the ensemble average of the corresponding Legendre moments

$$a^{(k)}(N,N') = \langle P_k(\cos\theta_{NN'})\rangle = \frac{1}{\mathcal{N}_{N'}}\sum_{i=1}^{\mathcal{N}_{N'}} P_k(\cos\theta^{(i)}_{NN'}) \quad (11)$$

where the sum runs over the ensemble of trajectories ending in a given N' rotational state.

Note that the above treatment is appropriate for QCT calculations in which OH(A) is treated as a closed shell molecule. QCT estimates of the "open shell" spin-rotation and hyperfine level changing cross sections and the associated polarization parameters were obtained using the tensor opacity formalism described in detail previously.[22] As long as the electron and/or nuclear spins can be considered as spectators, this method allows the determination of depolarization cross sections, $\sigma^{(k)}_{j\rightarrow j'}$ with $k > 0$, even in the case of elastic collisions. The only classical cross sections that cannot be converged are those for "pure" elastic collisions with $k = 0$, and in which no angular momentum transfer takes place and N and j do not change. However, these pure elastic cross sections of rank $k = 0$ do not contribute to the depolarization cross sections.

Calculations were also carried out for some sample initial states in which the collision energy was varied in a single batch of trajectories. The method to determine $\sigma_{N\rightarrow N'}(E_{coll})$ has been described in refs 37 and 38 and with specific application to the present problem in ref 21. The collision energy dependence of the depolarization parameters $a^{(k)}(N,N';E_{coll})$ can also be evalu-

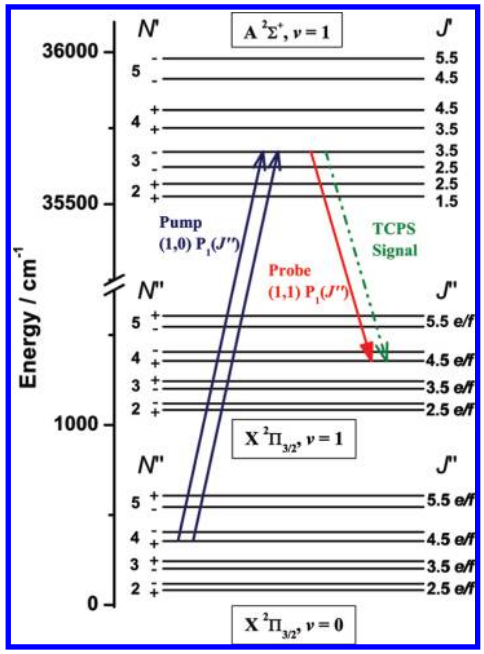

Figure 1. Schematic diagram of rotational energy levels for OH($X^2\Pi$, $v = 0$, 1) and OH($A^2\Sigma^+$, $v = 1$) relevant to TCPS signal generation. For clarity, energy-level splittings are not shown to scale. The Λ-doublet splitting in OH($X^2\Pi_{3/2}$) and the spin-rotation splitting in OH($A^2\Sigma^+$) are both considerably exaggerated; the vibrational spacing in OH($X^2\Pi$) is reduced. The upper $X^2\Pi_{1/2}$ spin−orbit manifold (F_2) has also been omitted for clarity. Example TCPS transitions, specific to this work, are indicated; the pump beam is resonant with the off-diagonal (1,0) $P_{11}(j)$ branch and the probe is resonant with the diagonal (1,1) $P_{11}(j)$ branch. This example would result in signal generation (broken arrow) from only the OH($A^2\Sigma^+$, $v = 1$, $j = 3.5$, f_1) level.

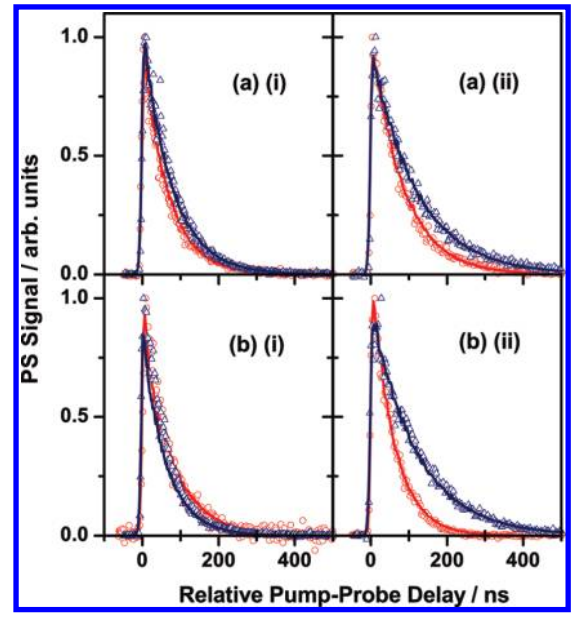

Figure 2. Example OH(A, $v = 1$) TCPS signals as a function of pump−probe delay. (a) $k = 1$ and (b) $k = 2$ (f_1 spin-rotation levels) for (i) $N = 1$ and (ii) $N = 4$. All decay traces were recorded with approximately 300 mTorr of collision partner Ar (red/gray) or He (blue/dark gray).

ated.[17] This allows determination of the thermally averaged depolarization cross sections $\langle\sigma_{N\to N'}^{(k)}\rangle$ by convoluting the energy dependent collision cross-section and depolarization parameters with the Maxwell−Boltzmann distribution. These thermally averaged depolarization cross sections can be compared directly with the experimentally determined values (see Section III).

B. Experimental Section. ***1. Polarization Spectroscopy Studies.*** Detailed descriptions of our experimental approach have been provided previously, including measures taken to eliminate the effects of unwanted stray magnetic fields.[11−16] The work described here employs a "Λ-shaped" two-color PS scheme[13] to measure the collisional removal of orientation and alignment moments for selected unique spin-rotation levels in OH($A^2\Sigma^+$, $v = 1$) (see Figure 1). All measurements were carried out at room temperature (nominally 295 K).

The OH(X) radical was generated via laser photolysis of nitric acid (60% w/w) at 193 nm in the presence of the collider gases He or Ar (both BOC Ltd.). To ensure that the translational distribution of the OH was thermalized and that any residual angular momentum polarization resulting from the photolysis had been lost, a time delay of 10 μs was introduced between photolysis and pump laser pulses. The pump laser was tuned to selected lines in the $A^2\Sigma^+ \leftarrow X^2\Pi$ (1,0) band (∼282 nm). Circular and linear pump polarizations were used to generate nonzero spherical tensor moments of rank $k = 1$ and $k = 2$, respectively, in the ground and excited state rovibrational levels resonant with the transition. The bulk polarization was interrogated by a linear probe pulse, using the same spectroscopic branch-type as the pump, but tuned to the $A^2\Sigma^+ \leftarrow X^2\Pi$ (1,1) band (∼314 nm). This scheme therefore resulted in TCPS signals, which copropagate with the probe but with the orthogonal polarization, that were generated exclusively from the excited OH($A^2\Sigma^+$, $v = 1$, N, f_1) levels. More specifically, the $^PP_{11}(N)$ branch was used to monitor the $k = 1$ moments and $^QQ_{11}(N)$ branch for the $k = 2$ moments. The reasons for these choices lie in the branch sensitivity for the different polarization moments, as we have described in detail previously.[13] Varying the relative pump−probe delay allowed the collisional evolution of the orientation and alignment moments to be monitored.

One potential experimental complication could arise from the presence of neighboring satellite lines when pumping and probing the $^QQ_{11}(N)$ spectroscopic branches. The centers of these transitions are separated by ∼0.3 cm^{-1}, which is comparable to the pump laser bandwidth. Because of the non-linear nature of PS, the polarization generated depends on the square of the pump fluence and transition linestrength, hence that prepared in the neighboring spin-rotation level (f_2) by the wing of the pump pulse is negligible. Scanning the probe laser (which has a narrower bandwidth, ∼0.15 cm^{-1}) while the pump was centered on $^QQ_{11}(N)$ indicated that there was no contribution to the PS signal from the f_2 spin-rotation level. We also recorded data using a mixed pump/probe scheme (pump $^QQ_{11}(N)$, probe $^PP_{11}(N)$), where the isolated $^PP_{11}(N)$ transitions ensure that the probe will only be sensitive to the f_1 spin-rotation level. This scheme provided the same k_{PS} values as pumping and probing $^QQ_{11}(N)$, giving further confidence in the method used to obtain the majority of the data. In principle, a further experimental artifact could arise from spontaneous fluorescence from the pumped $A^2\Sigma^+$ level which populates OH($X^2\Pi$, $v = 1$) with some degree of polarization. If so, this would produce a contribution to the TCPS signal from the lower state with which the probe is resonant. However, given the relatively long time scales for fluorescence (radiative lifetime ∼700 ns) and the dilution over quantum levels in the lower state, this contribution was assessed to be negligible.

2. Data Analysis: Polarization Spectroscopy Data. Examples of typical TCPS pump−probe delay traces are provided in Figure 2 and demonstrate the excellent signal-to-noise ratios that are achieved. The general form of the delay trace is a rise dependent on the pump and probe laser temporal bandwidths,

followed by an exponential decay. We note that the pronounced quantum beats present in our previous experiments on OH(X) are not visible in OH(A). This is the result of the substantially larger (several hundred megahertz) hyperfine splitting in OH(A), which cannot be resolved by our nanosecond laser pulses (see also Section IIB3). The traces were fitted using the theoretical description of TCPS previously derived by us.[13] In brief, TCPS is a variant of four wave mixing in which the interaction of the pump (twice) and probe beams with the sample generates a third-order nonlinear polarization that then radiates a signal beam, the fourth wave. Various different time-orderings of the pump and probe beams can contribute to the observed signal, and each can be represented by a Feynman diagram that may be used to direct a perturbative treatment of the signal electric field. The result can be expressed as

$$[\boldsymbol{P}^{(3)}(t)\cdot\varepsilon_4^*] = C\Phi \sum_k F(\epsilon_1\epsilon_2\epsilon_3\epsilon_4;k)G(J_iJ_eJ_f;k)\mathrm{e}^{-\Gamma_k^{J_eJ_e}\tau_2} \tag{12}$$

Here C is a term describing the dependence of the signal on population of the initial state, transition line strength and the pump and probe electric field magnitudes, and Φ describes the phase dependent terms in the signal electric field. $F(\epsilon_1\epsilon_2\epsilon_3\epsilon_4;k)$ depends on the polarizations of the four photons involved, while $G(J_iJ_eJ_f;k)$ is the product of 6-j symbols describing the sensitivity to spectroscopic branch. The final term is the exponential decay with rate, $\Gamma_k^{J_eJ_e}$, of the prepared bulk polarization during the delay period, τ_2, between the second and third photons. These last three terms are dependent on the tensor rank, k, and when the probe beam is delayed after the pump beam, only $k = 1$ is nonzero for circular polarized pump light, and $k = 2$ for linear pump light.

Experimentally, we measure the intensity of the signal beam, which is the cycle average of the square modulus of the electric field. This results in the signal depending on the square of the population of the initial level and of the pump beam intensity, and pump/probe transition line strengths, as well as introducing a strong transition polarization sensitivity through the 6-j symbols.[13]

To accurately model the full TCPS signal, it is necessary to integrate contributions of the different time-ordered interactions over the temporal pulse shapes of the pump and probe lasers. This is performed numerically by a Monte Carlo approach for an assumed decay rate, providing a predicted TCPS signal. The decay rate $\Gamma_k^{J_eJ_e}$ is varied iteratively to minimize the χ^2 deviation between experiment and simulation. The observed decay rates were assumed to have the form

$$\Gamma_k^{J_eJ_e} = k_{\mathrm{int}}^{(k)} + k_{\mathrm{PS}}^{(k)}[\mathrm{M}] \tag{13}$$

where $k_{\mathrm{int}}^{(k)}$ is the (tensor dependent) intercept rate representing all nonbimolecular loss processes (see Section IIIB). The desired TCPS bimolecular rate constants, $k_{\mathrm{PS}}^{(k)}$, were extracted from measurements at multiple collider number densities, [M], with the whole measurement cycle repeated on different days for several rotational levels to ensure reproducibility of the results. The bimolecular rate constants derived from the TCPS experiments may be written

$$k_{\mathrm{PS}}^{(k)} = k_{\mathrm{RET}} + k^{(k)} \tag{14}$$

that is, the rate constants determined in the TCPS experiments represent the sum of the RET rate constants out of an initial state j, $k_{\mathrm{RET}} \equiv \sum_{j'} k_{j\rightarrow j'}$, and the pure elastic depolarization rate constants, $k^{(k)}$. Equation 14 may be rewritten in terms of the thermally averaged cross sections

$$\sigma_{\mathrm{PS}}^{(k)} = \sigma_{\mathrm{RET}} + \sigma^{(k)} \tag{15}$$

Equations 14 and 15 assume that population loss is dominated by RET. Collisional population loss could also take place by quantum-state changing inelastic vibrational and electronic energy transfer. However, previous studies of inelastic transfer within OH(A) have shown that both vibrational[39,40] and electronic energy transfer[40−43] are relatively inefficient for He and Ar with total removal rate constants that are 1 or 2 orders of magnitude less than that for RET. Therefore, to a good approximation $k_{\mathrm{PS}}^{(k)}$ represents the sum of rotationally inelastic scattering (including pure spin-rotation-changing transitions, with $\Delta N = 0$, $\Delta j = \pm 1$) and pure elastic depolarization (with $\Delta N = \Delta j = 0$).

We have considered and eliminated the possibility that the PS decay traces are affected by repopulation of the pumped level through multiple collisions. Using the calculated state-to-state population transfer-rate constants, we determine that the fraction of molecules returning to the initially prepared level, after suffering two collisions, was approximately 10−20%. Within a Poisson model, this would result in a deviation from exponential behavior by a maximum of 15%. This is similar to our experimental uncertainties. More importantly, to have this maximum effect the returning molecules must retain their initial polarization after two collisions. On the basis of the QCT predictions that there is substantial depolarization accompanying inelastic collisions for OH(A) + Ar, we believe that any effect on the observed PS decay of the pumped level will be negligible. We also find no evidence for nonexponential decay for OH(A) + He data, and as we show below the PS data closely match the predicted behavior for RET, so we again believe that any effects of collisional repopulation are not significant.

3. Zeeman Quantum Beat Studies. The experimental procedures for determining depolarization cross sections from ZQBS have also been described previously,[17−19] and only a brief summary will be given here. OH(X) was generated by pulsed 248 or 193 nm photodissociation of hydrogen peroxide.[44−52] H_2O_2 flowed in a 50:50 mixture with water through the reaction chamber at a constant partial pressure of ≲20 mTorr. Electronically excited OH(A) radicals in $v = 0$ were obtained at a fixed photolysis-probe laser delay of 9 μs by pulsed excitation of OH(X) using the (0−0) band of the A←X transition. The experiments were performed with Nd:YAG-pumped dye laser probe radiation (bandwidth ∼0.36 cm^{-1} in the UV), in counter-propagating laser beam geometry. The minimum pressure of collider gas (Ar) used was kept above ∼50 mTorr, sufficient to allow translational moderation of OH(X) down to 300 K. The collider gas, Ar, flowed into the chamber through a separate inlet valve to allow experiments to be performed over a range of partial pressures from ∼50 to ∼1500 mTorr. The OH(A) spontaneous fluorescence was passed through a set of polarizing optics (see below), and the emission was then dispersed using a monochromator, before being detected with a UV-sensitive photomultiplier. With this method, it is possible to monitor transitions from single rotational states and, in particular, to separate the elastic depolarization contribution from that of RET collisions. The fluorescence decay traces were recorded on a

TABLE 1: Lines of the (0-0) Band of the OH(A) ← OH(X) Transition Used in the ZQBS Experiments[a]

excitation line	detection line	peak width (Å)	overlapping lines ($\Delta\lambda$)
		Alignment	
$Q_{11}(1)$	$Q_{11}(1)$	1.00	$Q_{21}(1)$ (0.04 Å)
$Q_{11}(2)$	$Q_{11}(2)$	1.00	$Q_{21}(2)$ (0.05 Å) $R_{22}(2)$ (0.28 Å)
$Q_{11}(4)$	$Q_{11}(4)$	1.00	$Q_{21}(4)$ (0.10 Å) $R_{22}(1)$ (0.77 Å)
$Q_{11}(5)$	$Q_{11}(5)$	1.00	$Q_{21}(5)$ (0.11 Å)
$R_{22}(7)$	$P_{22}(9)$	2.00	$P_{12}(9)$ (0.19 Å) $O_{12}(6)$ (0.23 Å)
$R_{11}(13)$	$P_{11}(15)$	2.00	
		Orientation	
$P_{12}(1)$	$P_{12}(1)$	1.00	$Q_{22}(7)$ (0.90 Å)
$P_{11}(2)$	$P_{11}(2)$	1.00	$Q_{11}(6)$ (0.95 Å)
$R_{22}(3)$	$R_{22}(3)$	1.40	
$R_{22}(4)$	$R_{22}(4)$	1.40	
$R_{22}(7)$	$P_{22}(9)$	1.70	$P_{12}(9)$ (0.19 Å) $O_{12}(6)$ (0.23 Å)
$R_{11}(13)$	$P_{11}(15)$	2.00	

[a] Note that the alignment measurements were made using Q-branch data, which has greater sensitivity to molecular alignment, but is overlapped with the satellite lines.

digital oscilloscope and transferred to a PC for subsequent data acquisition and analysis. The response time of the system was determined to be $\lesssim$20 ns. A complete list of transitions employed, together with the monochromator resolutions, is given in Table 1 (for the notation used see ref 53).

A Glan-Taylor polarizer was used to improve the polarization of the frequency doubled dye laser radiation immediately prior to entering the reaction chamber, and the purity of the polarization was determined to be better than 95% on exiting the chamber. In the case of alignment measurements, a photoelastic modulator was used to switch the probe laser linear polarization either 90° to the fluorescence detection direction or parallel to it on alternate laser shots. The polarizer used for detection was aligned parallel to the probe laser propagation axis. The photolysis laser radiation was used without polarization. In the case of orientation measurements, the probe radiation was switched between left and right circularly polarized light on alternate laser shots using a photoelastic modulator. A quarter waveplate followed by a Glan-Taylor polarizer were placed in front of the entrance slits of the monochromator.

The ZQBS experiments were performed in a uniform magnetic field of between 0 and 50 Gauss. The field was produced using a pair of matched Helmholtz coils, which were placed inside the reaction chamber, about 2.5 cm away from the interaction region. As in our previous work,[17−19] the center of the reaction chamber was screened from external magnetic fields by μ-metal shielding. The field was checked using a Hall probe, but could also be determined from the Zeeman beat frequency, since the g_F values for OH(A) are known quite precisely.[54−61] For the alignment experiments, the axis of the magnetic field was aligned parallel to the fluorescence detection direction, while for the orientation experiments the field was directed orthogonal to the fluorescence detection axis and the probe laser propagation axis. Full details of the orientation measurements have been presented in a recent publication.[19]

4. Data Analysis: Zeeman Quantum Beat Studies. Full details of the analysis of the ZQBS data has been presented previously.[17−19] The nonzero nuclear magnetic moment of the H-atom nucleus ($I = 1/2$) splits the rotational levels of OH($A^2\Sigma^+$) into two hyperfine components, characterized by the total angular momentum $\boldsymbol{F} = \boldsymbol{I} + \boldsymbol{j}$. The applied magnetic field lifts the degeneracy of the magnetic sublevels of each of these hyperfine components (Zeeman splitting) resulting in $2F + 1$ components characterized by the quantum number M_F (the projection quantum number along the magnetic field direction). The dye laser employed in the present work has a pulse duration of ~5 ns, and hence quantum beats between levels split by more than ~30 MHz will be unobservable. The energy splitting between the two hyperfine states of OH(A) with different F quantum numbers is of the order of several hundred MHz,[62,63] hence only the beats between Zeeman components of the individual hyperfine sublevels are observed in the present study (see further below).

In the case of alignment measurements, the fluorescence decays with Zeeman quantum beats can be described using the following expression[54−56,60]

$$I = A\mathrm{e}^{-k_p t} \times [1 + \mathrm{e}^{-k_d t} \sum_F C_F \cos(2\pi\alpha_F H t + \phi)] \tag{16}$$

In this equation, H is the magnetic field strength, ϕ is the phase of the beat signal, defined by the probe laser and detector polarization geometries, and A and C_F are constants defining the total intensity and the relative beat amplitudes, respectively. In the present experiments, in which hyperfine beats are not resolved, the relative beat amplitudes, C_F, include a term to allow for hyperfine depolarization,[64] and vary only slightly with F for the levels probed. In the Hund's case (b) limit, appropriate to OH($A^2\Sigma^+$), the parameter α_F, which defines the beat frequency per unit applied field, can be written to a good approximation[54−56,60]

$$\alpha_F \simeq 2\frac{\mu_0}{h} g_F \tag{17}$$

with

$$g_F = g_j \frac{F(F+1) + j(j+1) - I(I+1)}{2F(F+1)} \tag{18}$$

and

$$g_j = g_e \frac{j(j+1) + S(S+1) - N(N+1)}{2j(j+1)} \tag{19}$$

g_e is the Landé g value for the electron, and the quantum numbers are those of OH(A) in its excited electronic state. The rotational alignment data were recorded with the probe laser polarization switched on alternate laser shots between parallel ($I_\parallel$) and perpendicular ($I_\perp$) configurations with respect to the detection polarization. In these experiments, the field direction is parallel to the detection direction, so a quantum beat is observed for $I_\parallel$, but not for $I_\perp$. For the data analysis, both $I_\perp$ and $I_\parallel$ can be represented by eq 16 employing the same parameters, but with a 180° phase difference. For $I_\perp$, the magnetic field, H, must also be set to zero. The alignment depolarization values presented are obtained by fitting the ratio $I_\parallel/I_\perp$, rather than fitting $I_\parallel$ separately, since this allows decoupling of the polarization decay from the population decay. The latter contains information about the RET cross sections, and these were obtained by fitting either the field-on only data, using eq 16, or by fitting field-off data, using $I_\parallel + 2I_\perp$, which is only sensitive to the population decay. As expected, to a good

approximation the two methods gave the same RET cross-section values.

In the case of orientation measurements, the term in the beat frequency, α_F, is reduced by a factor of 2.[19] Furthermore, it is the difference between the signals obtained using left and right circularly polarized light (I_L and I_R, respectively) that is fit with the expression

$$\mathcal{O} = \frac{I_L - I_R}{I_L + I_R} = e^{-k_d t} \sum_F C'_F \cos(2\pi\alpha'_F H t + \phi) \tag{20}$$

with $\alpha'_F = \alpha_F/2$ to obtain the disorientation rate constants. The summed data $I_L + I_R$ was used to obtain the RET cross sections. In principle, these summed signals have a very small quantum beat arising from rotational alignment, which has twice the frequency of the orientation beat. In practice, the present experiments were insufficiently sensitive to observe this quantum beat, although it could be allowed for in the RET cross-section analysis by fitting using eq 16.

Two phenomenological first order rate constants, k_p and k_d, have been introduced to allow for decay of the population and the angular momentum polarization, respectively.[65,66] The rate constants are dependent on the concentration of the collider, and can both be expressed as sums of rate constants describing collision-free and collisional-induced decay processes[17−19]

$$k_p = k_0 + k_1[M] \tag{21}$$

$$k_d = k_2 + k_3[M] \tag{22}$$

The population decay, characterized by k_p, is associated with processes that remove OH(A), such as fluorescence (k_0) or electronic quenching (k_1). As with the TCPS measurements, in the present ZQBS experiments in which a single emission transition is resolved RET is the main contributor to the collisional population loss, k_1. This is because electronic quenching is negligible under the conditions employed.[40−43] k_2 is associated with depolarization in the absence of a collider gas, M, which could arise, for example, from magnetic field inhomogeneities.[15,18] As discussed previously,[17,18] the k_2 values observed at the fields employed here, typically $\sim 1 \times 10^6$ s^{-1}, were around half the loss rates due to fluorescence, and thus can be regarded as a relatively minor decay channel. Of particular interest to the current work is k_3 (or the related thermally averaged cross section, $\langle\sigma_3\rangle$), which accounts for the elastic depolarization of OH(A). Unlike the TCPS data, the ZQBS cross sections do not include a contribution from RET and to distinguish the various cross sections we label the collisional disorientation and "disalignment" cross sections and rate constants from the ZQBS experiments $\sigma^{(1)}_{ZB}$ and $\sigma^{(2)}_{ZB}$, and $k^{(1)}_{ZB}$ and $k^{(2)}_{ZB}$, respectively. The experimental collisional depolarization rate constants $k^{(k)}_{ZB}$ are closely related to the pure elastic depolarization rate constants, $k^{(k)}$ defined in Section IIA2. The fact that the two quantities are not identical is something that has been discussed previously.[17,18] It arises because the states populated during collisional relaxation have different g_F values and hence have different precession frequencies in the magnetic field. In the case that the emission transition is not resolved, this can lead to an unwanted dephasing of the beat signal. However, in the majority of the present experiments, in which a single emission transition is resolved, this dephasing effect has been shown by detailed simulation to be of minor importance. Dephasing in the present experiments could arise because of population of different hyperfine levels on collision (i.e., collisions in which $\Delta F \neq 0$ but $\Delta j = \Delta N = 0$). These states of different F have different g_F values and, hence, precession frequencies in the magnetic field. However, detailed simulations have shown that the g_F values for states with the same j and N are generally sufficiently similar to make this dephasing effect of very minor importance under the conditions of the present study, and it can be safely neglected within the error limits of the present experiments. Full details of the simulation procedures employed have been presented previously.[17]

For each rovibronic transition, a series of between 6 and 8 fluorescence decay curves obtained as a function of collider concentration (determined by the range of Ar partial pressures given in the previous section) were fitted globally, using the signal amplitudes, A, the relative beat amplitudes, C_F, the magnetic field H, the phase ϕ, and the four rate coefficients as adjustable parameters. Errors were estimated using a Monte Carlo error routine described elsewhere.[67] Typical data are shown in Figure 3.

III. Results

A. Zeeman Quantum Beat Results. ***1. Rotational Energy Transfer.*** Fluorescence decays derived from the sum of those recorded with left and right circularly (or orthogonal linearly) polarized probe radiation were fit to obtain the thermally averaged cross sections for RET out of the populated levels of OH(A, $v = 0$), $N = 0$, 1, 4, 5, 8, and 14. Similar data were obtained for $N = 4$ and $N = 5$ from the alignment quantum beat experiments, but the low N decays from the latter studies were not used because of complications due to unresolved satellite lines, as discussed further below. The RET data from the orientation and alignment experiments are shown in Table 2 and Figure 4, where they are compared with the results of the present QCT (see Table 3) and QM calculations. The agreement between the open shell QCT and o-s QM results is very good, as noted in our previous theoretical studies of this system.[17,21,22] The calculated RET cross sections are also close to the coupled states QM results published previously by Esposti and Werner, obtained using their own CEPA PES.[68] The calculated RET cross sections agree very well with the results of the experiments, although for the f_1 spin-rotation levels with $N = 0$ and 1 the latter are a little smaller than the theoretical values (see below).

There have been a number of previous experimental studies of RET cross sections for this system.[69,70] Unlike the present work, these were resolved into final rotational state. However, by summing the previous cross sections over final rotational state, j', a direct comparison with the current data can be made. These are shown for comparison as the black points in Figure 4. The present results are in excellent agreement with those from the more recent study by Jörg et al.[70] The earlier work of Lengel and Crosley[69] yielded data for the f_1 spin-rotation levels that are significantly lower than our measurements and also fall well below the present theoretical cross sections. In the present analysis, only the first 100 ns of the decays were employed in the fits at low N in order to avoid complications with significant back-transfer of population into the initially populated rotational levels on the time scale of the experiments through secondary collisions. Significant back transfer of population into the originally populated state might be a possible cause of the

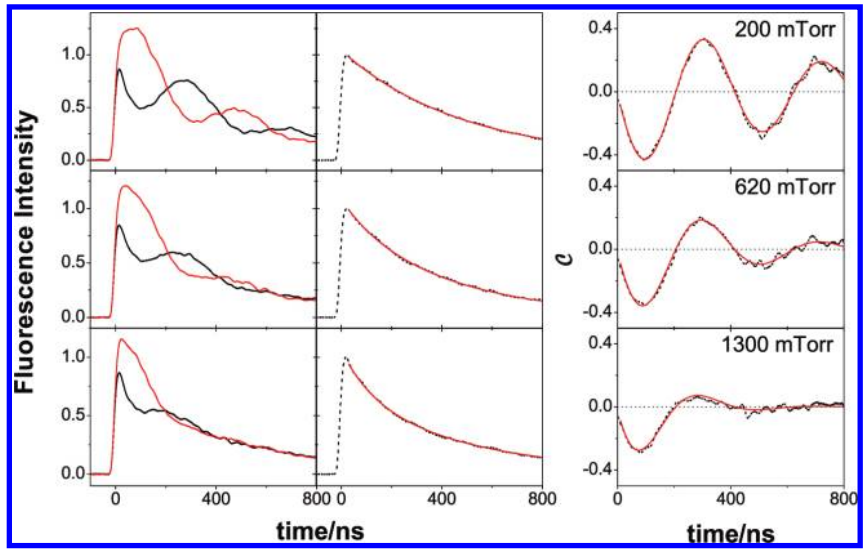

Figure 3. Example decays for ZQBS experiments on OH(A) + Ar. The data were recorded subsequent to excitation on the $R_{11}(13)$ line, with the emission detected from the $P_{11}(15)$ line, at the three pressures indicated. Left panels: the signals obtained with left and right circularly polarized light. Middle panels: the population decay obtained by summing the signals obtained with left and right circularly polarized light. Right panels: the decay of the orientation quantum beat, $\mathcal{C}$, as given by eq 20. The loss of the beat structure reflects pure elastic depolarization.

TABLE 2: Experimentally Determined Thermally Averaged (300 K) Cross Sections for Rotational Energy Transfer (σ_{RET}/Å^2, where $\sigma_{RET} \equiv \Sigma_{j'}\sigma_{j\to j'}$) and for Elastic Depolarization ($\sigma_{ZB}^{(k)}$/Å^2) of OH(A, $v = 0$) by Ar for Loss of Orientation ($k = 1$) and Loss of Alignment ($k = 2$)[a]

N	j	σ_{RET}	$\sigma_{ZB}^{(1)}$	$\sigma_{ZB}^{(2)}$
0	0.5	30.2 ± 6.7	0.0 ± 3.3	
1	1.5	35.8 ± 5.6	12.0 ± 5.5	35.3 ± 7.5
2	2.5			30.5 ± 4.3
4	3.5	32.1 ± 6.2	13.0 ± 5.0	
4	4.5	28.1 ± 5.1		32.7 ± 9.0
5	4.5	28.6 ± 6.9	18.1 ± 4.6	
5	5.5	26.8 ± 7.0		31.8 ± 9.4
8	7.5	16.6 ± 6.4	17.9 ± 3.5	30.3 ± 13.7
14	14.5	6.8 ± 3.2	15.7 ± 2.9	21.8 ± 14.6

[a] Note that in the ZQBS experiments the depolarization cross sections do not include a contribution from RET. The error bars were determined using a Monte Carlo procedure and represent 95% confidence limits.

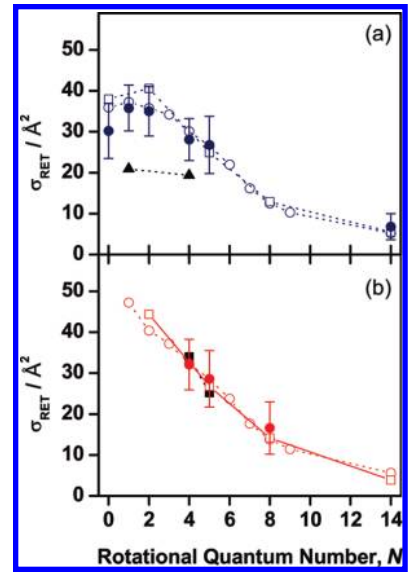

Figure 4. Cross sections for RET for OH(A, $v = 0$) + Ar: (a) from f_1 spin-rotation levels; (b) from f_2 spin-rotation levels. The data from the ZQBS experiments (filled points with 2σ errors) are compared with the present open shell QCT (open circles) and o-s QM (open squares) calculations at a fixed energy of 0.039 eV. In (a) the results from the work of Lengel and Crosley,[69] again summed over final state, are shown as black triangles. Similarly, in (b) the black squares are from the previous work of Jörg et al., summed over final rotational states.[70]

discrepancy between the two data sets for $N = 1$, although it seems less likely to be the explanation for the discrepancy for $N = 4$.

2. Collisional Disorientation. In the upper panel of Figure 5, we show the results of the ZQBS study of the elastic disorientation cross sections. Selected data for both f_1 and f_2 states of OH(A, $v = 0$) are presented for depolarization by Ar. We emphasize that these cross sections do not include contributions from RET. Apart from the very lowest rotational state of the f_1 manifold, the experiments suggest a value for loss of orientation of around 15 Å^2, almost independent of N. Note that the f_1, $j = 0.5$ level cannot show collisional angular momentum disorientation because only electron (and nuclear) spin contribute to the angular momentum, and both spin angular momenta are spectators to the collision to a very good approximation.[21,22] Overall, the QCT theoretical data are in broad agreement with the experimental results, although they underestimate the experimental values by around 10−20%.

The elastic depolarization of f_2 spin-rotation levels is predicted to be more efficient than for the f_1 levels, particularly at low N. Simple geometrical arguments suggest that if electron spin is a spectator, such that its direction in space remains unchanged during collision, then a given change in the direction $\boldsymbol{N}$ will lead to greater depolarization of $\boldsymbol{j}$ for f_2 spin-rotation levels, for which $j = N - S$, than for f_1 spin-rotational levels, for which $j = N + S$. As noted above, we have shown previously that both electron and nuclear spin can be treated very reliably as spectators in this system.[17,21,22]

3. Collisional Disalignment. The lower panel of Figure 5 shows the result of the collisional disalignment measurements for the f_1 levels of OH(A, $v = 0$) by Ar using ZQBS. These data are somewhat complicated at low N by the presence of unresolved satellite lines. The effect of this is to make the experiment additionally sensitive to collisions that change the spin-rotation state, but leave N unchanged, weighted by the appropriate line strength of the satellite lines. The disalignment cross

TABLE 3: Fixed Energy (E_{coll} = 0.039 eV) QCT Calculated Open Shell RET (σ_{RET}/Å^2) and Pure Elastic Depolarization Cross Sections ($\sigma^{(k)}$/Å^2) for OH(A) + Ar[a]

	f_1 levels ($j = N + 1/2$)			f_2 levels ($j = N - 1/2$)		
N	σ_{RET}	$\sigma^{(1)}$	$\sigma^{(2)}$	σ_{RET}	$\sigma^{(1)}$	$\sigma^{(2)}$
0	36.0	0.0				
1	37.3	9.6	23.3	47.3	16.4	
2	35.8	9.4	21.4	40.4	14.7	25.1
3	34.2	9.3	20.4	37.2	12.8	23.3
4	30.1	9.9	21.6	32.3	13.0	24.3
5	26.5	11.3	24.3	28.5	14.2	26.7
6	22.0	12.8	27.7	23.7	15.8	30.2
7	13.4	14.0	30.8	14.6	17.1	33.7
8	10.1	14.1	31.6	11.1	16.9	34.7
9	8.3	13.3	30.7	9.2	15.8	33.9
14	4.2	8.6	22.2	4.5	9.8	24.6

[a] As with the Zeeman quantum beat data, the depolarization cross sections do not include a contribution from RET. Note that the calculations employ an OH(A) bond length fixed at its equilibrium value. Typical errors are better than 5%.

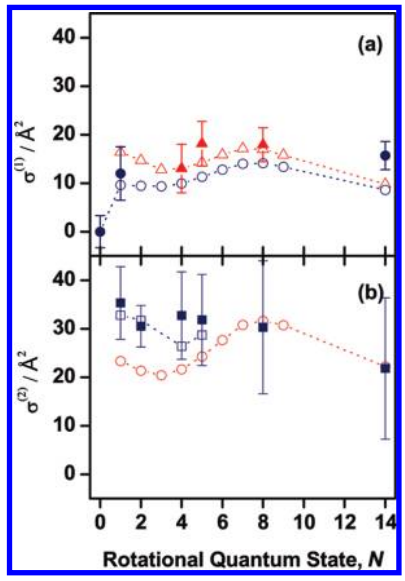

Figure 5. (a) OH(A, $v = 0$) + Ar pure elastic disorientation cross sections from the ZQBS experiments (filled symbols with error bars). The data are resolved into f_1 (circles) and f_2 (triangles) spin-rotation states. The open shell QCT data are shown as open symbols. (b) As for panel (a) but showing data for OH(A, $v = 0$) + Ar pure elastic disalignment cross sections from the ZQBS experiments. The open shell QCT cross sections for pure elastic disalignment are shown as the open circles, specifically for the f_1 spin-rotation levels. The open squares are fits to simulated data that include the effects of overlapping satellite lines (see text). The measured disalignment cross sections are therefore enhanced by the depolarization caused by spin-rotation collisions, weighted by the satellite line strength. The effect of unresolved satellite lines is negligible for $N = 8$ and 14.

sections for inelastic spin-rotation changing collisions are relatively large for OH(A) + Ar, typically of the order of 10 Å^2.[21,22] These spin-rotation changing collisions also lead to significant extra dephasing, because the g_F values for f_1 and f_2 levels have different signs.[17,18] To allow for these effects, we have performed a detailed simulation of the alignment experiments using the QCT cross sections, and including, with appropriate weighting, the effects of inclusion of unresolved satellite lines. The results of these simulations are also shown in the lower panel of Figure 5, alongside the QCT estimates of the pure elastic ($N = N'$ and $j = j'$) disalignment cross sections. The simulations account very well for the experimental data, although as with the orientation data they slightly underestimate

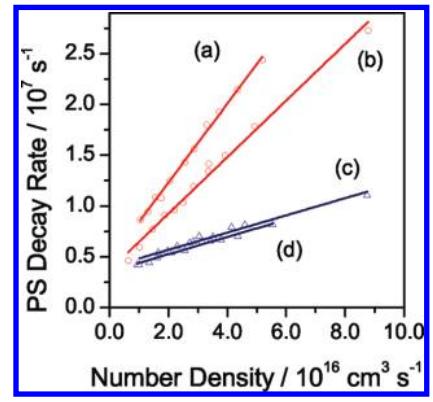

Figure 6. Representative plots of the measured TCPS decay rate as a function of collision partner number density. All data are for OH(A, $v = 1$) $N = 4$ (f_1 spin-rotation level). (a) Ar, $k = 2$; (b) Ar, $k = 1$; (c) He, $k = 2$; (d) He, $k = 1$.

the experimental values, this time by around 5−10% on average. At high N (i.e., $N = 8$ and 14) the satellite lines are very weak, and the experimental measurements essentially yield the true elastic disalignment cross sections. From the ZQBS experimental and theoretical data shown in Figure 5 we can conclude that the pure elastic disalignment cross sections for OH(A) + Ar, like those for disorientation, are essentially independent of N, and take values of around 25 Å^2.

There has been one previous measurement of the elastic depolarization of OH(A) by Ar from the work of Brinkman and Crosley.[71] They obtained a value of 20 Å^2 for the f_1 $N = 4$ level, which is in excellent agreement with the results of the QCT calculations for pure elastic disalignment. However, one caveat about these measurements is that Brinkman and Crosley employed a technique that involved observing the time dependence of the ratio of Q_{11} and P_{11} emission intensities, and it is unclear the extent to which the effects of satellite lines, and spin-rotation changing collisions, were allowed for in these experiments.

B. Polarization Spectroscopy Results. Returning to the data shown in Figure 2, the main empirical observation from the TCPS signals is that the OH(A, $v = 1$) traces in the presence of Ar or He decay considerably more rapidly for Ar than for He at the same pressure. Differences between rotational levels and between the different polarizations are visually less obvious from these single-pressure measurements but were determined by systematic determination of the decay rates as a function of the collider gas partial pressure in the range 100−2800 mTorr. Figure 6 illustrates the satisfactory linearity of such plots. The significant positive intercept, represented by $k_{int}^{(k)}$, is expected, and can be decomposed into various effects. Spontaneous fluorescence makes a minor contribution that was absent from our previous measurements on OH(X), but nevertheless the intercept is largely dominated by collisions with the precursor (HNO_3/H_2O). Its magnitude is consistent with the expected high efficiency of a number of inelastic and reactive processes at the known partial pressures of precursor used in this work (typically 10−20 mTorr). The absolute values are larger for alignment compared to orientation measurements.

The quantities of primary interest here are the phenomenological bimolecular rate constants, $k_{PS}^{(k)}$, for each of the tensor ranks $k = 1$ and 2, which correspond to the slopes in Figure 6, and similar plots. Figure 6 confirms our principal observations that these total PS removal rate constants, which, recall from above, to a good approximation represent the sum of the elastic depolarization and RET rate constants (see eq 14), are greater

TABLE 4: Thermally Averaged (300 K) Cross Sections ($\sigma_{PS}^{(k)}$/Å^2) for Collisional Depolarization of OH(A, $v = 1$, f_1) by He[a]

N	j	$\sigma_{PS}^{(1)}$	$\sigma_{PS}^{(2)}$
0	0.5	18.9 ± 2.0	
1	1.5	16.5 ± 1.4	19.4 ± 2.0
2	2.5	11.8 ± 1.4	11.5 ± 0.9
3	3.5	11.3 ± 1.9	8.6 ± 0.7
4	4.5	5.8 ± 0.8	6.1 ± 1.0
5	5.5	7.9 ± 1.4	4.9 ± 1.1

[a] The data were obtained using TCPS. Note that these cross sections represent the sum of the RET cross sections and the pure elastic depolarization cross sections, as defined by the equivalent of eq 15.

TABLE 5: Thermally Averaged (300 K) Cross Sections ($\sigma_{PS}^{(k)}$/Å^2) for Collisional Depolarization of OH(A, $v = 1$, f_1) by Ar[a]

N	j	$\sigma_{PS}^{(1)}$	$\sigma_{PS}^{(2)}$
0	0.5	30.6 ± 3.3	
1	1.5	41.7 ± 5.5	43.8 ± 4.8
2	2.5	31.6 ± 4.0	53.2 ± 4.5
3	3.5	39.8 ± 4.9	47.9 ± 3.8
4	4.5	42.4 ± 2.3	52.8 ± 4.8
5	5.5	40.0 ± 4.1	42.4 ± 3.4

[a] The data were obtained using TCPS. Note that these cross sections represent the sum of the RET cross sections and the pure elastic depolarization cross sections, as defined by the equivalent of eq 15.

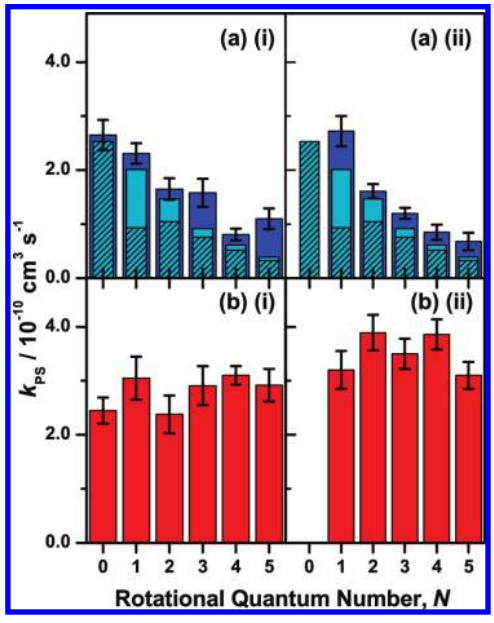

Figure 7. Measured TCPS rate constants, $k_{PS}^{(k)}$ defined in eq 14, for OH(A, $v = 1$), f_1 spin rotation levels for (a) He and (b) Ar with (i) $k = 1$ and (ii) $k = 2$. Error bars represent 95% confidence limits. The panels shown in (a) also include the CS o-s QM RET rate constants calculated by Jörg et al.[72] in which the contributions from pure spin-rotation changing collisions (i.e., those with $\Delta N = 0$ but $\Delta j = \pm 1$) are highlighted in unshaded light blue (light gray). The remaining shaded bar represents the sum of all other inelastic processes, as calculated by Jörg et al.[72]

for Ar than for He and that the difference between orientation and alignment measurements is more pronounced for Ar. The data for all levels and both collision partners are summarized in Tables 4 and 5, and represented graphically in Figure 7.

For He, $k_{PS}^{(k)}$ declines smoothly as a function of N, for both $k = 1$ and $k = 2$. As an example, $k_{PS}^{(2)}$ is a maximum for $N = 1$ (2.72×10^{-10} cm^3 s^{-1}) and falls monotonically by a factor of ~4 at $N = 5$ (0.68×10^{-10} cm^3 s^{-1}). We note that the spherical tensor moment of rank $k = 2$ is zero, by definition, for the $N = 0$, f_1 level with $j = 1/2$; this state cannot be aligned and so no alignment decay rate constant is reported. The values for $k_{PS}^{(1)}$ are broadly similar to $k_{PS}^{(2)}$. For several rotational levels ($N = 2$, 3 and 5) $k_{PS}^{(1)}$ apparently exceeds $k_{PS}^{(2)}$, but we presume this is simply due to experimental fluctuations, and that the data overall are consistent with at most a minor contribution from elastic depolarization.

Also shown in the panels for OH(A, $v = 1$) + He is a comparison with the RET rate constants obtained in the coupled-states QM calculations of Jörg et al.[72] Note that these calculations were performed with an OH(A) bond length set to the average for that of OH(A, $v = 0$). The theoretical data are also resolved into pure spin-rotation changing collisions and are discussed further in Section IV. The calculated RET rate-constants[72] follow the experimental TCPS data very closely. It seems reasonable to infer from this that RET and depolarization are not particularly sensitive to OH(A) vibrational state and, more importantly, that elastic depolarization plays only a minor role in the loss of polarization signal for OH(A, $v = 1$) + He.

In contrast with the experimental data for He, for OH(A, $v = 1$) + Ar the magnitude of $k_{PS}^{(k)}$ is more nearly constant across the range of N investigated. The values in Table 5 show pronounced differences between orientation and alignment, with $k_{PS}^{(2)}$ larger than $k_{PS}^{(1)}$ for all N. This implies unambiguously that there must be a significant contribution from elastic depolarization, confirming the observations from the ZQBS experiments.

As with the ZQBS experiments, for OH(A) + Ar it is possible to make a direct comparison between the present QCT theoretical calculations and the results of the TCPS studies. As noted above, the latter are sensitive to the sum of the RET cross sections and those for pure elastic depolarization, as expressed by eqs 14 and 15. Figure 8 compares the cross sections obtained for OH(A, $v = 1$) + Ar from the TCPS experiments with the sum of the RET and pure depolarization cross sections determined in the QCT calculations, which employ an OH(A) bond length fixed at r_e. Also included in this figure are the experimental RET cross sections obtained in the ZBQS experiments for OH(A, $v = 0$) + Ar. In addition, for future reference, we also show the QCT calculated contribution to the RET cross sections from pure spin-rotation changing collisions (for which $\Delta j = \pm 1$, $\Delta N = 0$). Overall, there is good agreement between the theoretical data and the TCPS measurements, suggesting that the depolarization behavior is not that sensitive to OH(A) vibrational state. The comparison also supports the conclusions of the ZQBS study that for OH(A) + Ar elastic depolarization provides an important collisional loss mechanism for rotational orientation and alignment, which is relatively insensitive to OH(A) rotational state.

C. Comparisons between the Two Sets of Experimental Cross Sections. By summing the RET and disorientation cross sections obtained from the ZQBS experiments it is possible to make a direct comparison with the results from the TCPS experiments (see eq 15). As shown in the upper panel of Figure 9, overall the agreement between the two data sets is excellent. Where direct comparison is possible, the ZQBS measurements appear slightly higher than the TCPS data, but note that for $N = 4$, 5 the ZQBS data are for the f_2 spin-rotation levels which have been shown in Section IIIA to tend to have slightly higher depolarization cross sections than the f_1 levels.

A similar comparison can also be made for the disalignment data. In this case direct comparison is a little more difficult to

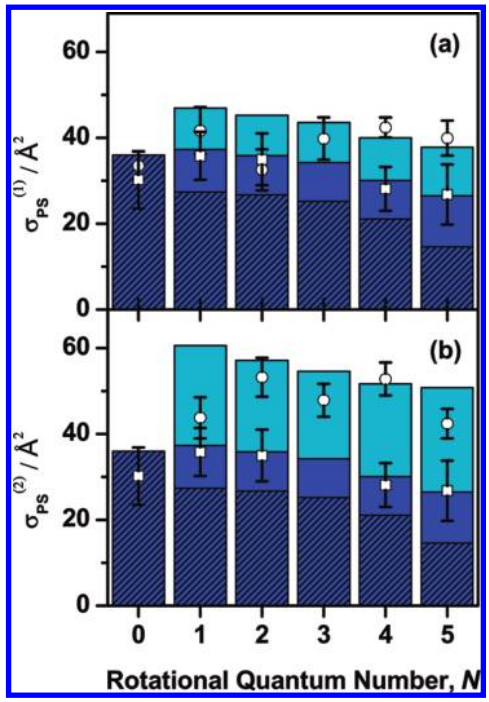

Figure 8. Comparison of thermally averaged cross sections obtained from the TCPS measurements, $\sigma_{PS}^{(k)}$ defined in eq 15, on OH(A, $v = 1$) (circles with error bars) and the open shell QCT calculations of the combination of RET (blue columns) and elastic depolarization (cyan columns) in OH(A, $v = 0$). (a) $k = 1$ and (b) $k = 2$. The open squares with error bars are the RET cross sections obtained from the ZQBS experiments. The open shell QCT RET data are resolved into pure spin-rotation changing cross sections (dark bars, unshaded), and the cross sections for the sum of all other inelastic processes (shaded bar).

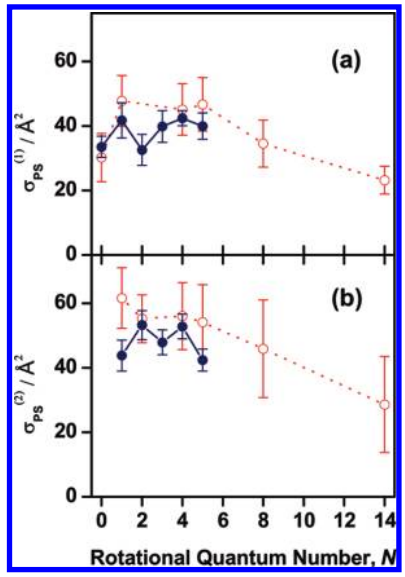

Figure 9. (a) Comparison between the OH(A, v) + Ar orientation data obtained from the TCPS (filled circles) and the ZQBS (open circles) experiments. The latter are the sum of the RET and disorientation cross sections, and neglect small differences in the values for f_1 and f_2. (b) As for the upper panel but showing a comparison of the alignment cross sections obtained in the two experiments. The alignment data have been corrected for the effects of spin-rotation changing collisions based on the simulations using the QCT cross sections (see text for details).

make because the ZQBS measurements also contain a contribution at low N from the depolarization cross sections of spin-rotation changing collisions. However, if we use the theoretical values of the latter to correct the ZQBS disalignment data, and then add the result to the ZQBS RET cross sections, the results are in good agreement with the TCPS measurements, as illustrated in the lower panel of Figure 9. As indicated by the data shown in Figure 5, the magnitude of the correction is around 10 Å^2 for $N = 1$, but falls to around 4.5 Å^2 for $N = 5$ and is negligible for $N = 8$ and 14, the decreasing importance of the correction reflecting the decrease in line strength of the partially overlapping satellite lines. The ZQBS alignment data is consistently a little higher than that obtained from the TCPS experiments, particularly for $N = 1$, but the differences are generally within the combined uncertainties in the data, particularly bearing in mind the complications surrounding the correction of the ZQBS alignment data for the effects of overlapping satellite lines.

It should be emphasized once more that the ZQBS measurements refer to OH(A) in $v = 0$, while the TCPS measurements to OH(A) in $v = 1$. The good agreement between the two data sets lends support to the view that the RET and depolarization cross sections are not very sensitive to the initial OH(A) vibrational state. It seems unlikely that any of the aforementioned differences in the two data sets could arise from the different vibrational levels employed, since, if anything, vibrational excitation might be expected to enhance the efficiency of collision depolarization.

The principal conclusion from the comparisons between the experiments and between experiment and theory is that for OH(A) + Ar elastic disorientation has a cross-section of between 10 and 15 Å^2, while elastic disalignment is around 20−30 Å^2, with both sets of depolarization cross sections being relatively insensitive to the initial rotational state.

IV. Discussion

A. Assessment of the Two Experimental Techniques. The comparisons between the results from the two experiments presented in the preceding section provide a useful guide to the strengths and weaknesses of the two methods. Because the TCPS experiments rely only on laser radiation for excitation and detection, they are inherently of higher resolution than the present ZQBS experiments, which involve dispersing the emission with a monochromator to isolate emission from a particular quantum state. Although double resonance variants of the ZQBS measurements would be possible in systems such as NO(A), which have additional fluorescent electronic states available into which polarization may be transferred with good resolution,[19] these double resonance methods would then lose one advantage of the current ZQBS experiments, that the polarization data is obtained effectively in a single shot.

Another advantage of ZQBS is that it probes separately both the population and polarization of the ensemble in a single experiment. That has proved of particular benefit in the present work to distinguish RET from pure elastic depolarization. In contrast, TCPS is only sensitive to the bulk polarization of the sample, and hence decays with both population and polarization loss. In principle, other related degenerate four wave mixing techniques provide mechanisms for the separate determination of population and polarization properties.[73,74] In practice however, with the nanosecond-pulsed lasers used in these experiments, such measurements would be dominated by other noncollisional processes arising from the formation of spatial gratings in the sample.[12] Laser-induced fluorescence-based techniques such as ZQBS almost certainly possesses higher sensitivity than TCPS, where the ultimate detection limit is determined by the extinction ratio of the polarizers (1×10^{-6} for the polarizers used in the experiments reported here). In

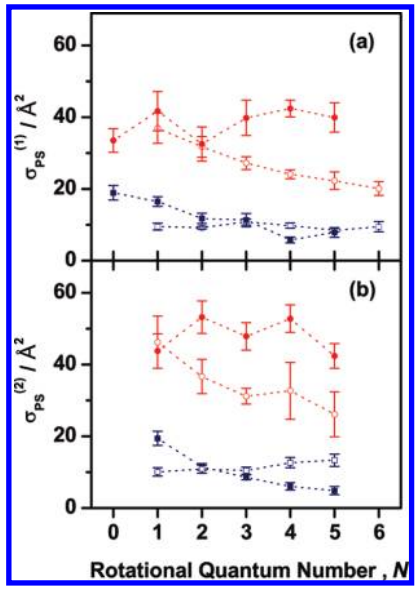

Figure 10. Comparison of measured TCPS thermally averaged cross sections for OH(A, $v = 1$) f_1 (filled symbols) and OH(X, $v = 0$) F_1 e (open symbols) for Ar (circles) and He (squares). (a) $k = 1$ and (b) $k = 2$.

addition, the nonlinear nature of the technique results in a squared dependence on the number density of the initial level. Despite this, TCPS does have some distinct advantages as well, in addition to that of resolution. A signal can only be generated if the sample is polarized, and no switching of the pump polarization is required.

It should be emphasized that, in spite of the respective strengths and weaknesses of TCPS and ZQBS, as far as can be judged from the present data, the two techniques appear to give results which are in excellent agreement with each other.

B. Comparison between OH(A) + He/Ar and OH(X) + He/Ar. As noted in the introduction, a considerable body of data has been assembled in recent years on the collisional depolarization of OH($X^2\Pi$) with a variety of collision partners, including He and Ar.[11−16] Comparison with the present data for OH(A) is particular instructive and is shown in Figure 10, which includes cross sections obtained from the TCPS experiments (i.e., assumed to be the combination of the RET and pure elastic depolarization cross sections, as given in eq 15) for the four systems OH(X) and OH(A) with He and Ar. At low N, the depolarization data for OH(X) and OH(A) with He and Ar are remarkably similar. As already observed, the depolarization data for OH(A) + Ar are distinctive in not decreasing significantly with N. For both OH(X) and OH(A), He is much less efficient as a depolarizing collider than Ar. This partly reflects kinematic effects arising from the fact that at fixed collision energy, or fixed temperature, He carries a smaller momentum than Ar. However, the PES is also likely to play some role, as discussed further in the following subsection.

It should be borne in mind that OH($X^2\Pi$) and OH($A^2\Sigma^+$) belong to different electronic terms, and that has a bearing on the types of inelastic processes that can occur in these two molecules. Collisions between OH(A) and the rare gases take place on a single PES.[75−77] Electron and nuclear spin can be treated reliably as spectators to the dynamics, and the cross sections for pure spin-rotation changing collisions are governed by the extent to which N is depolarized during collision.[21,22,75−77] Because OH(A) + Ar collisions tend to be more depolarizing than OH(A) + He, spin rotation changing collisions play a more significant role in the former system, particular at higher N.[22,68] Recall that the cross sections for pure spin-rotation changing collisions obtained in the QCT calculations for OH(A) + Ar have been presented in Figure 8. In the case of OH(A) + He collisions, the efficiency of spin-rotation changing collisions falls very rapidly with increasing N, as shown in the upper panels of Figure 7, which include the theoretical cross-section data for pure spin-rotation changing collisions from Jörg et al.[72]

On the other hand, collisions between OH(X) and the rare gases are controlled by two PESs, an A′ and an A″ PES.[78] In the Hund's case (a) limit, transitions between OH(X) spin−orbit states take place on a difference potential, $V_{diff} = (V_{A''} - V_{A'})/2$, while transitions within a given spin−orbit state are governed by an average potential, $V_{sum} = (V_{A''} + V_{A'})/2$. Furthermore, in the same limit, the latter is also responsible for transitions between OH(X) Λ-doublet levels, and these play an important role in RET collisions between OH(X) and Ar, particularly at low N.[24,25] (Note, however, that these predictions should no longer be considered entirely quantitatively accurate.[79]) By contrast to OH(X) + Ar, Λ-doublet changing transitions in OH(X) + He collisions are much less important.[25] Very recent work by Dagdigian and Alexander has indicated that V_{diff} plays a surprisingly important role in the elastic depolarization of OH(X) + Ar, but a more minor role in the case of NO(X) + Ar.[26] This indicates that the Hund's case (a) approximation is insufficient for the purposes of explaining the depolarization behavior of OH(X), which is well known to be an intermediate case at low N and proceed quite rapidly toward case (b) as N increases.

In light of the above discussion, it could be argued that a fairer reflection of the depolarizing nature of the OH(X)-Rg and OH(A)-Rg PESs would be to compare the pure elastic depolarization cross sections for the ground state with the sum of the depolarization cross sections for pure elastic and pure spin-rotation changing collisions for the excited state. In the case of OH(A) + Rg, the sum would better reflect the depolarization of N. In fact, the sum of the cross sections is exactly equal to the closed shell elastic depolarization cross-section in the limit that electron spin is a spectator.[21] In Figure 11 we compare the calculated elastic depolarization cross sections obtained by Dagdigian and Alexander for OH(X) + Ar using o-s QM methods[24] with both the closed and open shell QCT depolarization data for OH(A) + Ar obtained in the present work. The figure illustrates clearly that once the depolarizing effects of spin-rotation changing collisions are included for OH(A) + Ar, the effective elastic depolarization cross sections for collision of Ar with the excited state of OH(A) are, on average, considerably larger than for collisions involving OH(X). For OH(A) + Ar the spin-rotation changing depolarization cross sections are typically around 10 Å^2, largely independent of N, and adding these to the elastic depolarization cross sections significantly enhances the "elastic" depolarization over that generated on the ground state PES. Of course, for the ground state of OH(X), the electron spin is coupled to the internuclear axis in the Hund's case (a) limit, and such a sum would be neither appropriate, nor possible.

Figure 11 also serves to reinforce one of the main conclusions of the present paper, that the elastic depolarization for OH(A) with Ar is essentially independent of N, while that for the OH(X) with Ar falls rapidly with N.

C. Role of the PES and the Mechanism of Elastic Depolarization. Despite the differences in the electronic terms of OH(X) and OH(A) it is instructive to consider the PESs for the four systems in question. In Figure 12, we plot the radial dependence of the Legendre moment expansion coefficients of

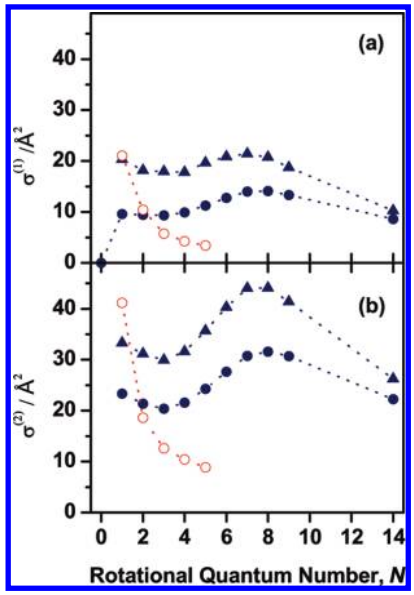

Figure 11. Comparison of calculated elastic depolarization cross sections for OH(A) + Ar (filled symbols) and OH(X) + Ar (open symbols), and for both (a) $k = 1$ and (b) $k = 2$. The OH(X) data are from Dagdigian and Alexander (o-s QM)[24] (although note also ref 79) and OH(A) data are from this work (open shell QCT). For OH(A) + Ar, the circles represent the pure elastic depolarization and the triangles the sum of elastic depolarization and spin-rotation changing depolarization (see text).

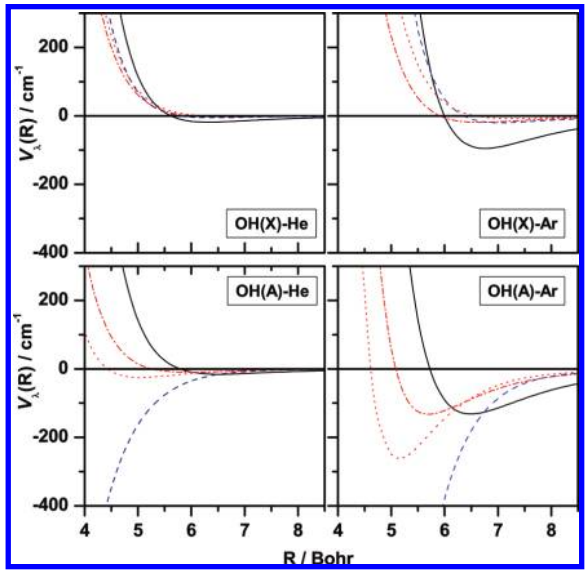

Figure 12. Ab initio PESs decomposed into Legendre components [$P_\lambda(\cos\theta)$] of order $\lambda = 1-3$. Plots for OH−He and Ar are shown for both OH(X) and OH(A), as indicated. The OH(X)−He data are taken from ref 80, the OH(X)−Ar data are from ref 16 (although note also ref 79), OH(A)−He are from ref 68, and the OH(A)−Ar data are taken from ref 21. Curves are for $\lambda = 0$ (black), $\lambda = 1$ (dashed-dotted red), $\lambda = 2$ (dashed blue), $\lambda = 3$ (dotted red).

the PESs for OH(X) with He and Ar (upper panels) and OH(A) with He and Ar (lower panels). In the case of OH(X) we use the expansion coefficients of the summed potential[78]

$$V_{\text{sum}}(R,\gamma) = \sum_{\lambda=0}^{\infty} V_\lambda(R) P_\lambda(\cos\gamma) \qquad (23)$$

A similar expansion of the potential can be defined for the systems involving OH(A).[75] The role of these expansion terms for OH(X) + He and Ar has recently been discussed in some detail by Dagdigian and Alexander,[25] and these arguments will not be repeated here. As mentioned above, it should also be emphasized that Dagdigian and Alexander have recently demonstrated that both V_{sum} and V_{diff} play a role in the elastic depolarization of OH(X) by Ar.[26] Nevertheless, it is immediately apparent on comparing the potentials for OH(X) with those for OH(A) that the latter are significantly more attractive and anisotropic.[79] In the case of OH(X) and OH(A) with Ar, reasons for the differences in the PESs have been discussed in detail by Esposti et al.[68] OH(A) with Ar can be thought of as forming an incipient chemical bond,[68,21] although electron correlation effects are known to play a large role in determining the majority of the binding energy.[68] Thus, for the excited OH(A)−Ar PES the well-depth exceeds 1000 cm^{-1},[21] while for OH(X)−Ar it is only of the order of 100 cm^{-1}.[16]

The isotropic $\lambda = 0$ terms in the potentials for OH(X) and OH(A) with the respective rare gases are remarkably similar (compare the solid lines in the upper and lower panels of Figure 12), but this isotropic term only leads to pure elastic scattering without leading to a change in polarization (i.e., in the absence of *M*-state changing collisions).[25,75,78] Changes in polarization require $\lambda > 0$, and for these terms there are striking differences between OH(X) and OH(A) with the rare gases, particularly with Ar. Most notable are the large magnitudes of the expansion coefficients for $\lambda = 1-3$ in the case of OH(A) + Ar, particularly for $\lambda = 2$. Within a direct, Born model of the scattering of a $^2\Sigma^+$ radical with the rare gases,[75] it is the dominant λ-even terms in the potential with $\lambda > 0$ that are responsible for both elastic depolarization and spin-rotation collisions in which $\Delta j = \pm 1$, but $\Delta N = 0$. Similar arguments have recently been used in the context of elastic depolarization of OH(X) by He and Ar.[25,78] Although a simple direct scattering model is almost certainly inappropriate for OH(A) + Ar, because of the presence of the deep potential energy well, these $\lambda > 0$ terms in the potential will still be the ones that largely dictate the elastic depolarization behavior. Given the very significant differences in these expansion terms in the PESs for OH(X) and OH(A), in particular with Ar, it might seem somewhat surprising that larger differences in the elastic depolarization are not evident. However, as already discussed, a fairer comparison between the elastic depolarization of OH(X) and OH(A) with Ar is made if one includes the depolarization by spin-rotation changing collisions in the elastic depolarization, as illustrated in Figure 11. With this comparison, it is clear that OH(A) + Ar becomes progressively more depolarizing than OH(X) + Ar as *N* increases.

D. Elastic versus Inelastic Depolarization in OH(A) + Ar. The most important effect of changing the PES appears to be manifest in the *N*-dependence of the elastic depolarization and RET cross sections, and on the relative contributions of Λ-doublet or spin-rotation changing collisions to RET. Previous ZQBS studies of the total depolarization of OH(A) by Ar show that it proceeds with cross sections which are significantly higher than those for RET.[17,21,22] There are two reasons for this. First, as shown in the present work, elastic depolarization contributes significantly to the total loss of polarization. Second, inelastic scattering leads to very efficient scrambling of the angular momentum polarization, essentially leading to a near complete loss of polarization in a single collision.[17,22]

A crucial factor in the balance between elastic and inelastic collisions, and in particular its *N*-dependence, is the approach geometry and how this influences the effects of rotational averaging. Elementary considerations show that inelastic collisions will be promoted most efficiently when the angular

momentum transferred from orbital to rotational motion lies parallel (or antiparallel) to *j*, which obviously corresponds to in-plane collisions. Equally, such in-plane collisions are incapable of causing elastic depolarization. For in-plane collisions, increasing *N* will cause a blurring of the anisotropy due to the deep wells on the OH(A) + Ar surface located at 0 and 180°, and hence reduce the efficiency of RET.

On the other hand, out-of-plane collisions are capable of causing both RET and elastic depolarization. The recent work of Dagdigian and Alexander[24,25] has shown that for OH(X) + Ar elastic depolarization is promoted by impact parameters that fall predominantly in the region between the inner wall and the attractive minimum in the potential. Together with the strong negative collision-energy dependence of the elastic depolarization cross sections which they have also demonstrated, this suggests that a significant component of the elastic depolarization is caused by "following"-type trajectories, where the attractive potential causes the Ar atom to drag the plane of OH(X) rotation around as it passes. For low-impact-parameter collisions perpendicular to the plane of rotation, rotational motion will in fact have little effect on the anisotropy of the potential because largely the less attractive, side-on geometries will be sampled. In these T-shaped configurations, as noted first by Esposti et al.,[68] the PESs for OH(X)−Ar and OH(A)−Ar are actually very similar. This suggests that these configurations do not play much of a role in elastic depolarization of either state, which is as expected anyway for purely mechanical reasons because of the relatively small torques that would be imparted. For higher impact parameters the situation is more complicated, but in the high-*N* limit the potential experienced will be the average over the full rotational cycle of the strongly attractive ends and less attractive sides of the OH molecule. For the present OH(A) + Ar system, we have discovered that efficient elastic depolarization is maintained to much higher *N*. Apparently, therefore, for OH(A) + Ar this rotational averaging is insufficient to suppress elastic depolarization, unlike the less anisotropic OH(X) + Ar system for which Dagdigian and Alexander have demonstrated that the efficiency of elastic depolarization declines very rapidly with *N*, as shown in Figure 11.

It would clearly be an interesting extension of this work to examine the partial cross sections, or opacity functions, for different elementary processes for the OH(A) + Ar system as Dagdigian and Alexander have done for OH(X) + rare gases[24−26] and indeed to explore the effects of correlations between plane of rotation and approach geometry on the outcomes of collisions of both OH(X) and OH(A) with simple partners and in other related collision systems.

V. Conclusions

Two color polarization spectroscopy has been used to measure the collision depolarization of OH(A, $v = 1$) by He and Ar. In the former system, collisional loss of both rotational orientation and alignment proceeds at a rate close to that for loss of population by RET, suggesting that elastic depolarization plays a modest role. For OH(A, $v = 1$) + Ar, on the other hand, much more efficient collisional loss of rotational polarization is observed, implying a significant role for elastic depolarization that remains almost constant with increasing *N*. The TCPS measurements for OH(A, $v = 1$) + Ar have been complemented by a set of ZQBS measurements for OH(A, $v = 0$) + Ar which have allowed the loss of population and polarization to be independently determined. These studies confirm that both elastic disorientation and disalignment are important in OH(A) + Ar, and have cross sections which are approximately independent of *N*. The experimental data from the two sets of experiments are shown to be in very good agreement with each other, and with the results of QCT calculations on a recently developed PES by Kłos et al.[21] At low *N*, elastic depolarization in OH(A) + Ar is comparable to that in OH(X) + Ar, despite the fact that the potential is an order of magnitude more attractive. However, for OH(A) + Ar the elastic disorientation and disalignment cross sections persist at around 10−20 Å^2 and 20−30 Å^2, respectively, essentially independent of *N*, whereas for OH(X) + Ar[24,25] they fall rapidly with *N*. We attribute these differences to the much greater anisotropy of the OH(A)−Ar potential combined with the requirement for elastic depolarizing collisions to occur via geometries with a component of the relative motion perpendicular to the plane of OH rotation.

Acknowledgment. The support of the U.K. EPSRC for support to K.G.M. and M.L.C. (through Grant EP/C015975/1) and to M.B. (via Programme Grant EP/G00224X/1) is gratefully acknowledged. M.L.C. also thanks the U.K. EPSRC for the award of an RCUK Academic Fellowship. This work has also been funded by the Ministry of Science and Innovation of Spain under Grant CTQ2008-02578/BQU.

References and Notes

(1) Lorenz, K. T.; Chandler, D. W.; Barr, J. W.; Chen, W.; Barnes, G. L.; Cline, J. I. *Science* **2001**, *293*, 2063.
(2) Alexander, M. H.; Davis, S. L. *J. Chem. Phys.* **1983**, *78*, 6754.
(3) de Miranda, M. P.; Clary, D. C. *J. Chem. Phys.* **1997**, *106*, 4509.
(4) Case, D. E.; Herschbach, D. R. *Mol. Phys.* **1975**, *30*, 1537.
(5) Kim, S. K.; Herschbach, D. R. *Faraday Discuss. Chem. Soc.* **1987**, *84*, 159.
(6) Cline, J. I.; Thomas Lorenz, K.; Wade, E. A.; Barr, J. W.; Chandler, D. W. *J. Chem. Phys.* **2001**, *115*, 6277.
(7) Wade, E. A.; Lorenz, K. T.; Chandler, D. W.; Barr, J. W.; Barnes, G. L.; Cline, J. I. *Chem. Phys.* **2004**, *301*, 261.
(8) Chandler, D. W.; Stolte, S. Inelastic energy transfer: The NO-rare gas system. In *Gas Phase Molecular Reaction and Photodissociation Dynamics*; Lin, K. C., Kleiber, P. D., Eds.; Transworld Research Network: Kerala, India, 2008.
(9) Costen, M. L.; Marinakis, S.; McKendrick, K. G. *Chem. Soc. Rev.* **2008**, *37*, 732.
(10) Gijsbertsen, A.; Linnartz, H.; Rus, G.; Wiskerke, A. E.; Stolte, S.; Chandler, D. W.; Kłos, J. *J. Chem. Phys.* **2005**, *123*, 224305.
(11) Crichton, H. J.; Costen, M. L.; McKendrick, K. G. *J. Chem. Phys.* **2003**, *119*, 9461.
(12) Costen, M. L.; Crichton, H. J.; McKendrick, K. G. *J. Chem. Phys.* **2004**, *120*, 7910.
(13) Costen, M. L.; McKendrick, K. G. *J. Chem. Phys.* **2005**, *122*, 164309.
(14) Marinakis, S.; Paterson, G.; Kłos, J.; Costen, M. L.; McKendrick, K. G. *Phys. Chem. Chem. Phys.* **2007**, *9*, 4414.
(15) Marinakis, S.; Paterson, G.; Richmond, G.; Rockingham, M.; Costen, M. L.; McKendrick, K. G. *J. Chem. Phys.* **2008**, *128*, 021101.
(16) Paterson, G.; Marinakis, S.; Costen, M. L.; McKendrick, K. G.; Kłos, J. *J. Chem. Phys.* **2008**, *129*, 074304.
(17) Brouard, M.; Bryant, A.; Chang, Y.-P.; Cireasa, R.; Eyles, C. J.; Green, A. M.; Marinakis, S.; Aoiz, F. J.; Kłos, J. *J. Chem. Phys.* **2009**, *130*, 044306.
(18) Brouard, M.; Bryant, A.; Burak, I.; Marinakis, S.; Quadrini, F.; Garcia, I. A.; Vallance, C. *Mol. Phys.* **2005**, *103*, 1693.
(19) Brouard, M.; Chadwick, H.; Chang, Y.-P.; Cireasa, R.; Eyles, C. J. *Phys. Scr.*, in press.
(20) Brouard, M.; Chadwick, H.; Chang, Y.-P.; Cireasa, R.; Eyles, C. J.; Via, A. O. L.; Screen, N.; Aoiz, F. J.; Kłos, J. *J. Chem. Phys.*, DOI: 10.1063/1.3212608.
(21) Kłos, J.; Alexander, M. H.; Brouard, M.; Eyles, C. J.; Aoiz, F. J. *J. Chem. Phys.* **2008**, *129*, 054301.
(22) Aoiz, F. J.; Brouard, M.; Eyles, C. J.; Kłos, J.; de Miranda, M. P. *J. Chem. Phys.* **2009**, *130*, 044305.
(23) Follmeg, B.; Rosmus, P.; Werner, H.-J. *J. Chem. Phys.* **1990**, *93*, 4687.
(24) Dagdigian, P.; Alexander, M. H. *J. Chem. Phys.* **2009**, *130*, 094303.
(25) Dagdigian, P.; Alexander, M. H. *J. Chem. Phys.* **2009**, *130*, 164315.
(26) Dagdigian, P.; Alexander, M. H. *J. Chem. Phys.* **2009**, *130*, 204304.

(27) de Miranda, M. P.; Aoiz, F. J.; Banares, L.; Rábanos, V. S. *J. Chem. Phys.* **1999**, *111*, 5368.
(28) de Miranda, M. P.; Aoiz, F. J. *Phys. Rev. Lett.* **2004**, *93*, 083201.
(29) de Miranda, M. P.; Aoiz, F. J.; Brouard, M.; Sáez-Rábanos, V. *J. Chem. Phys.* **2004**, *121*, 9830.
(30) Alexander, M. H.; Manolopoulos, D. E.; Werner, H.-J.; Follmeg, B.; with contributions from Vohralik, P. F.; Lemoine, D.; Corey, G.; Johnson, B.; Orlikowski, T.; Berning, A.; Degli-Esposti, A.; Rist, C.; Dagdigian, P.; Pouilly, B.; van der Sanden, G.; Yang, M.; de Weerd, F.; Gregurick, S.; Kłos, J. Hibridon 4.3 (2009) is a package of programs for the time-independent quantum treatment of inelastic collisions and photodissociation. http://www.chem.umd.edu/groups/alexander/hibridon/hib43/.
(31) Manolopoulos, D. E. *J. Chem. Phys.* **1986**, *85*, 6425.
(32) Alexander, M. H.; Manolopoulos, D. E. *J. Chem. Phys.* **1987**, *86*, 2044.
(33) Hutson, J. M.; Green, S. *The MOLSCAT computer code*, version 14; Collaborative Computational Project No. 6 of the Science and Engineering Research Council: United Kingdom; 1994.
(34) Aoiz, F. J.; Verdasco, J. E.; Herrero, V. J.; Rábanos, V. S.; Alexander, M. H. *J. Chem. Phys.* **2003**, *119*, 5860.
(35) Bonnet, L.; Rayez, J.-C. *Chem. Phys. Lett.* **2004**, *397*, 106.
(36) Bañares, L.; Aoiz, F. J.; Honvault, P.; Bussery-Honvault, B.; Launay, J. M. *J. Chem. Phys.* **2003**, *118*, 565.
(37) Aoiz, F. J.; Bañares, L.; Díez-Rojo, T.; Herrero, V. J.; Rábanos, V. S. *J. Phys. Chem.* **1996**, *100*, 4071.
(38) Aoiz, F. J.; Banares, L.; Herrero, V. J. *J. Chem. Soc., Faraday Trans.* **1998**, *94*, 2483.
(39) Lengel, R. K.; Crosley, D. R. *J. Chem. Phys.* **1978**, *68*, 5309.
(40) Paul, P. H.; Durant, J. L., Jr.; Gray, J. A.; Furlanetto, M. R. *J. Chem. Phys.* **1995**, *102*, 8378.
(41) Williams, L. R.; Crosley, D. R. *J. Chem. Phys.* **1996**, *104*, 6507.
(42) Paul, P. H. *J. Quant. Spectrosc. Radiat. Transfer* **1994**, *51*, 511.
(43) Becker, K. H.; Haaks, D.; Tatarczyk, T. *Chem. Phys. Lett.* **1976**, *25*, 564.
(44) Gericke, K. H.; Klee, S.; Comes, F. J.; Dixon, R. N. *J. Chem. Phys.* **1986**, *85*, 4463.
(45) Grunewald, A. U.; Gericke, K. H.; Comes, F. J. *J. Chem. Phys.* **1988**, *89*, 345.
(46) Dixon, R. N.; Nightingale, J.; Weston, C. M.; Yang, X. *Chem. Phys. Lett.* **1988**, *151*, 328.
(47) Gericke, K. H.; Gläser, H. G.; Maul, C.; Dixon, R. N. *J. Chem. Phys.* **1990**, *92*, 411.
(48) Docker, M. P.; Hodgson, A.; Simons, J. P. *Faraday Discuss. Chem. Soc.* **1986**, *82*, 25.
(49) August, J.; Brouard, M.; Docker, M. P.; Hodgson, A.; Milne, C. J.; Simons, J. P. *Ber. Bunsen-Ges. Phys. Chem.* **1988**, *92*, 264.
(50) Brouard, M.; Martinez, M. T.; Milne, C. J.; Simons, J. P. *Chem. Phys. Lett.* **1990**, *165*, 423.
(51) Alexander, A. J. *Phys. Rev. A* **2002**, *66*, 060702.
(52) Alexander, A. J. *J. Chem. Phys.* **2003**, *118*, 6234.
(53) Luque, J.; Crosley, D. R. *Vol. LIFBASE: Database and simulation program*, version. 1.6; SRI International Report MP 99-009; 1999. http://www.sri.com/psd/lifbase/.
(54) Lebow, P.; Raab, F.; Metcalf, H. *Phys. Rev. Lett.* **1979**, *42*, 85.
(55) Raab, F.; Bergman, T.; Lieberman, D.; Metcalf, H. *Opt. Lett.* **1980**, *5*, 427.
(56) Raab, F.; Bergman, T.; Lieberman, D.; Metcalf, H. *Phys. Rev. A* **1981**, *24*, 3120.
(57) Carter, R. T.; Povey, I. M.; Bitto, H.; Huber, J. R. *J. Chem. Phys.* **1996**, *104*, 5365.
(58) Xin, J.; Reid, S. A. *J. Chem. Phys.* **2000**, *112*, 10067.
(59) Xin, J.; Reid, S. A. *J. Chem. Phys.* **2002**, *116*, 525.
(60) Xin, J.; Ionescu, I.; Kuel, D.; Reid, S. A. *Chem. Phys.* **2003**, *291*, 61.
(61) German, K. R.; Zare, R. N. *J. Chem. Phys.* **1971**, *54*, 4039.
(62) ter Meulen, J. J.; Majewski, W. A.; Meerts, W. L.; Dymanus, A. *Chem. Phys. Lett.* **1983**, *94*, 25.
(63) ter Meulen, J. J.; Ubachs, W.; Dymanus, A. *Chem. Phys. Lett.* **1986**, *129*, 533.
(64) Kummel, A. C.; Sitz, G. O.; Zare, R. N. *J. Chem. Phys.* **1988**, *88*, 7357.
(65) Brucat, P. J.; Zare, R. N. *J. Chem. Phys.* **1983**, *78*, 100.
(66) Brucat, P. J.; Zare, R. N. *J. Chem. Phys.* **1984**, *81*, 2562.
(67) Brouard, M.; Burak, I.; Gatenby, S. D.; Hart, D.; Minayev, D. *J. Chem. Phys.* **1999**, *110*, 11335.
(68) Esposti, A. D.; Werner, H.-J. *J. Chem. Phys.* **1990**, *93*, 3351.
(69) Lengel, R. K.; Crosley, D. R. *J. Chem. Phys.* **1977**, *67*, 2085.
(70) Jörg, A.; Meier, U.; Kohse-Höinghaus, K. *J. Chem. Phys.* **1990**, *93*, 6453.
(71) Brinkman, E. A.; Crosley, D. R. *J. Phys. Chem. A* **2004**, *108*, 8084.
(72) Jörg, A.; Esposti, A. D.; Werner, H.-J. *J. Chem. Phys.* **1990**, *93*, 8757.
(73) Williams, S.; Rahn, L. A.; Zare, R. N. *J. Chem. Phys.* **1996**, *104*, 3947.
(74) Wasserman, T. A.; Vaccaro, P. H.; Johnson, B. R. *J. Chem. Phys.* **1998**, *108*, 7713.
(75) Alexander, M. H. *J. Chem. Phys.* **1982**, *76*, 3637.
(76) Corey, G. C.; McCourt, F. R. *J. Phys. Chem.* **1983**, *87*, 2723.
(77) Corey, G. C. *J. Chem. Phys.* **1984**, *81*, 2678.
(78) Alexander, M. H. *J. Chem. Phys.* **1982**, *76*, 5974.
(79) Kłos, J. Private communication, 2009. It has been discovered following the submission of the present manuscript that a trivial but numerically significant error had been made in the construction of the PES for the OH(X)−Ar system reported in ref 16 by Paterson et al. A preliminary re-analysis indicates that the calculated population transfer rate constants are slightly increased on the corrected surface. There will also be some effect, expected to be similarly modest, on the elastic depolarisation cross sections of Dagdigian and Alexander.[24−26] The most noticeable effect on the radial dependence of the Legendre expansion coefficents is a slight shift of the $\lambda = 1$ term to longer range. These corrections do not materially alter any of the qualitative conclusions arrived at in the current paper, based on much larger differences between the OH(X)−Ar and OH(A)−Ar potentials.
(80) Lee, H.-S.; McCoy, A. B.; Toczylowski, R. R.; Cybulski, S. M. *J. Chem. Phys.* **2000**, *113*, 5736.

JP905348C